Structure Optimization of FePt Nanoparticles of Various Sizes for Magnetic Data Storage

M. TANASE, J.-G. ZHU, C. LIU, N. SHUKLA, T.J. KLEMMER, D. WELLER, and D.E. LAUGHLIN

Surfactant-coated, fcc disordered FePt nanoparticles of three different sizes between 3 and 7 nm were prepared and washed according to a modified reaction route based on Sun *et al.*[1] Hexane dispersions of nanoparticles were dried on transmission electron microscopy (TEM) grids, and the resulting monolayers were annealed by a sinter-free procedure at 600 °C and at 650 °C for 2 hours, respectively, developing the $L1_0$ phase while preserving their monodispersity. The order parameter of the $L1_0$ phase was measured using electron diffraction from statistically large ensembles of nanoparticles using an X-ray-like signal collection technique. The order parameter increases with particle size and with the temperature in the range 600 °C to 650 °C, being close to unity for the 7.2-nm particles annealed at 650 °C for 2 hours.

DOI: 10.1007/s11661-006-9081-6

I. INTRODUCTION

CHEMICALLY synthesized self-assembled FePt nanoparticles have been proposed as magnetic recording media that could be thermally stable beyond 1 Tbit/in^2.[1] However, in order for the potential of this kind of media to be realized, many requirements must be addressed, such as long storage time, uniaxial crystallographic texture, self-assembly over large areas, and a narrow distribution of switching fields. The long storage time and high storage density can be achieved in high magnetocrystalline anisotropy materials such as the $L1_0$ phase of FePt. The chemical route typically produces FePt nanoparticles in the fcc disordered state, and subsequent annealing is needed to induce the chemical ordering transformation into the high magnetocrystalline anisotropy $L1_0$ phase.* While annealing is a route for the phase transformation fcc $\rightarrow$ $L1_0$, it also promotes sintering and grain growth, which destroy the self-assembly. Various methods aimed at avoiding sintering have been reported, such as rapid thermal annealing,[2] *in-situ* thermal annealing,[3] preannealing of surfactant,[4] inert coatings followed by annealing,[5] epitaxial growth at high temperatures (500 °C[6]) or low temperatures (230 °C[7]), metal additives for the reduction of the ordering temperature,[8] covalent bonding with the substrate,[9] salt matrix annealing,[10] and direct $L1_0$ production in high boiling point solvents.[11] Another problem associated with annealing is incomplete phase transformation due to the dependence of the transformation temperature on particle size. Several workers have suggested that FePt does not order below a critical size of 3 nm in nanoparticles and 4 nm in granular thin films.[12] More recent work on granular thin films[13] has succeeded in inhibiting grain growth of particles of 3.5-nm average size, but without the formation of the $L1_0$ phase in particles smaller than 4 nm. We report the phase transformation fcc $\rightarrow$ $L1_0$ in particles of 3.2-nm diameter and also in single-crystal grains contained within these particles, which pushes the critical size for ordering below 3 nm, if such limit exists.

Cubic nanoparticles faceted on {100} planes are advantageous in that they may naturally lie on these planes, which helps the crystallographic alignment of the [001] easy axis along the sample normal. In the paradigm of the ultrahigh density perpendicular data storage using bottom-up principles (self-assembly), this alignment is important for the simultaneous achievement of uniform size and periodicity of bits (*i.e.*, nanoparticles) and the perpendicular alignment of the magnetic easy axis. Past studies on FePt nanoparticles focused on truncated octahedrons primarily faceted on {111} and {100} planes.[14] More recently, Zeng *et al.*[15] demonstrated shape-controlled synthesis and shape-induced texture in cubic $MnFe_2O_4$ nanoparticles, faceted along {100} planes. The same group produced cubelike FePt nanoparticles[16] and achieved

*For a list of methods of achieving the phase transformation fcc $\rightarrow$ $L1_0$ other than thermal annealing, refer to Ref. 20 (Sections 1.3 and 4.2.3).

M. TANASE, formerly with the Data Storage Systems Center, Carnegie Mellon University, is with the Argonne National Laboratory, Lemont, IL, USA Contact e-mail: tanase@anl.gov J.-G. ZHU and D.E. LAUGHLIN are with the Data Storage Systems Center, Carnegie Mellon University, Pittsburgh, PA 15213, USA C. LIU, formerly with Seagate Research, is with the Nanosys Inc., Palo Alto, CA 94304, USA N. SHUKLA, formerly with Seagate Research, is with the Institute for Complex Engineered Systems, Carnegie Mellon University, Pittsburgh, PA, USA T.J. KLEMMER and D. WELLER are with Seagate Research, Pittsburgh, PA, USA

This article is based on a presentation made in the symposium entitled "Phase Transformations in Magnetic Materials", which occurred during the TMS Annual Meeting, March 12–16, 2006, in San Antonio, Texas, under the auspices of the Joint TMS-MPMD and ASMT-MSCTS Phase Transformations Committee.

shape-controlled {100} texture and shape-controlled self-assembly in FePt nanocubes.[17]

The present study reports results on the phase transformation in nanoparticles with sizes between 3 and 7 nm and various shapes, including cubes with (100) facets, in which the unwanted sintering effect has been eliminated during thermal annealing by a novel procedure. As a notable difference with respect to previous thermal annealing procedures, long annealing times of the order of 2 hours and temperatures up to 650 °C are permitted, which in turn yield measurable crystallographic order parameters for large (10^3 to 10^4) ensembles of nanoparticles. Electron microscopy imaging is used to verify the area subject to measurements in its entirety for the absence of sintering. The analysis of the crystallographic texture and of the order parameter as a function of particle size and the initial texture is carried out using quantitative analysis of the selected-area diffraction signal in a manner similar to X-ray analysis.

II. EXPERIMENTAL DETAILS

Surfactant-coated, fcc disordered FePt nanoparticles of three different sizes (3.2, 5.7, and 7.2 nm) were synthesized according to a modified reaction route based on Chen *et al.*[17] and described in Shukla *et al.*[18] A typical synthesis route starts with 0.5 mmol of platinum (II) acetylacetonate and 1.0 mmol of iron pentacarbonyl in 20 mL of dichlorobenzene in the presence of 4.0 mmol of oleic acid and 4.0 mmol of oleylamine. The temperature is increased slowly until 169 °C to 170 °C after which the reaction is stopped and the particle solution can be exposed to ambient conditions for purification. The particles can be precipitated when a polar solvent such as ethanol is added, and the particles can be well redispersed into an nonpolar solvent such as hexane with the desired particle concentration. The transmission electron microscopy (TEM) specimens are prepared by dropping the particle solution onto a carbon grid. Hexane solutions of nanoparticles were dispersed on TEM grids (carbon type A, product 01820 from Ted Pella, Inc., P.O. Box 492477, Redding, CA 96049-2477). Upon drying, the nanoparticles form self-assembled layers of different coherence lengths. Hexane dispersions of nanoparticles were dried on TEM grids, and the resulting monolayers were annealed by a new sinter-free procedure at 600 °C and at 650 °C for times comprised between 30 minutes and 2 hours. The TEM specimens were annealed in an AG heat pulse rapid thermal annealer under high-purity argon flow, with a heating rate of 120 °C/s. The specimens were cooled in an inert gas flow and reached room temperature in approximately 15 minutes. The self-assembly, particle size, and crystallographic structure were investigated before and after annealing in a PHILIPS EM420T microscope with a point resolution of 3.5 Å operating at 120 kV. The order parameter of the nanoparticle samples was determined as follows. Selected area electron diffraction (SAED) patterns were collected digitally as 8-bit grayscale tagged image file format (.tiff) images with a resolution of 72 dpi and were azimuthally integrated using the Process Diffraction v. 2.1.7 software,[19] producing an intensity *vs* reciprocal distance distribution. A corresponding integrated intensity pattern collected from the specimen substrate only was obtained for each SAED pattern and numerically subtracted from it, to account for the diffuse scattering produced by the substrate.

The intensity integrated background SAED pattern, as shown in Figure 1(a), exhibits two low, broad peaks corresponding to the first and second spheres of interaction within the amorphous carbon substrate. Figure 1(b) illustrates the background subtraction procedure from the integrated SAED signal.

In the annealed samples, care was taken to include only monolayers in the selected area aperture, and the nanoparticles within the aperture were verified visually prior to taking the SAED patterns to ensure the absence of sintering. The sintering prevention method, which enables the development of the $L1_0$ phase in monolayers of monodispersed nanoparticles, is described by Tanase[20] and will be published

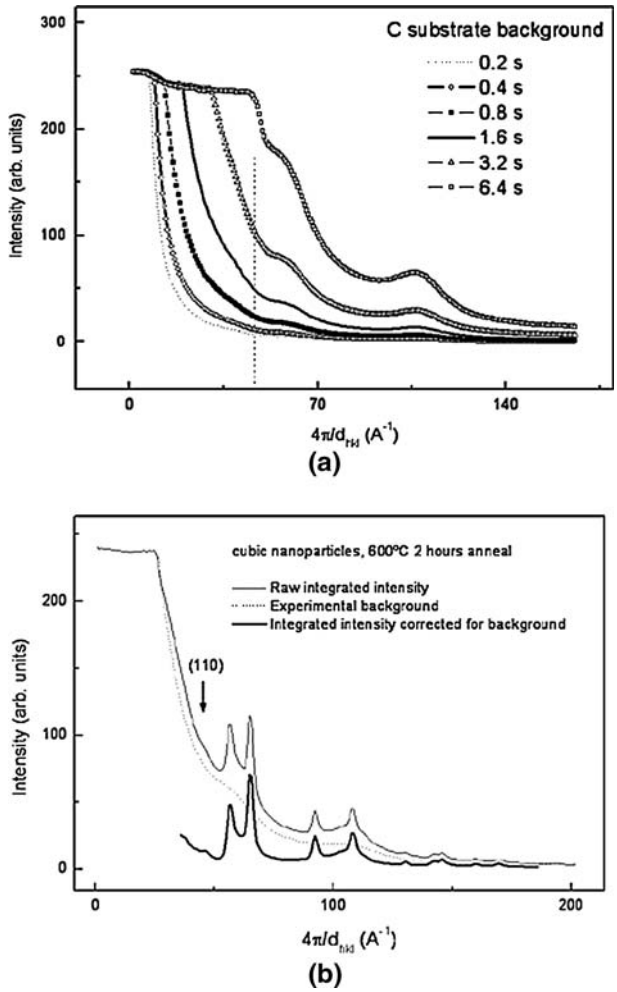

Fig. 1—(*a*) Carbon substrate contribution to the integrated-intensity SAED patterns, at different exposures. The vertical line marks the position of the (110) peak of the $L1_0$ structure. (*b*) Subtraction of the background produced by the amorphous carbon substrate from the integrated intensity SAED of the nanoparticles.

elsewhere. The SAED micrographs used in the determination of the order parameter have been taken from areas between 1.1 and 5.7 μm in diameter comprising 10^3 to 10^5 nanoparticles.

The order parameter for an atomically ordered binary crystal structure can be defined as[21]

$$S = \frac{r_A^\alpha - r_B^\alpha}{r_{A+b}^\alpha} \quad [1]$$

where r_A^α is the fraction of A atoms sitting on the "right" lattice site (of type α) and with r_B^α the fraction of B atoms sitting on the "wrong" lattice site (of type α). In the $L1_0$ structure, the α and β sites correspond to the Fe and Pt sites, respectively, in an ideal, fully ordered structure.

Experimentally, the order parameter is measured using the intensities of a pair of superlattice and fundamental reflections as[21]

$$S_{1v} = \left(\frac{I_s/I_f}{I_s^0/I_f^0}\right)^{1/2} \quad [2]$$

where I_s is the measured intensity of the superlattice peak, I_f is the measured intensity of the corresponding fundamental peak, and I_s^0 and I_f^0 are the correspondent intensities in the case of complete order ($S = 1$). A numerical value of $S = 1$ signifies that the present phase is fully ordered, whereas a value of 0 signifies that the phase is completely disordered. This formula, widely used in X-ray crystallography, is applicable to electron diffraction as well, with a few precautions: a proportional count detector should be employed, so that the intensity values are directly proportional to the amount of the phase; the intensities measured should be integral quantities rather than peak-height intensities, because the same reasons for peak broadening apply in TEM as in X-ray diffraction (*i.e.*, nonmonochromaticity of the beam, strain, and small particle size); a proper background subtraction must be performed prior to assigning numerical values to the peak intensities; and the texture of the material must be known and taken into account. The pair of superlattice-fundamental reflections chosen here to quantify the order parameter is (110) and (220). The Gatan charge-coupled digital (CCD) camera was employed as the proportional detector, and the background subtraction was performed as described previously. The denominator of Eq. [2] was calculated theoretically following Vainshtein[22] as

$$I_{hkl} = K\|\Phi_{hkl}\|^2 d_{hkl}^2 p \quad [3]$$

where I_{hkl} is the theoretical intensity of reflection (hkl), K is a proportionality constant, Φ_{hkl} is the structure factor of (hkl), d_{hkl} is the plane spacing, and p is the multiplicity.

Theoretical intensities in the case of complete disorder ($S = 0$) and complete order ($S = 1$) for various axial textures, calculated with Eq. [3], are listed in Tables I and II. The term I_{110} signifies theoretical intensity in axial texture [110], *etc.* The term p_{110} signifies the multiplicity of the given (hkl) plane in axial texture $<110>$, *etc.*

From Table II, the value of the denominator of Eq. [2] is 1.78, which is independent of a particular axial texture or combination of axial textures. The numerator of Eq. [2], however, is an experimental quantity, which can be affected by texture. We consider cubic nanoparticles with (100) facets, which exhibit an ideal (100) texture, as shown in Figure 2.

The easy axis distributes equally along three perpendicular directions, one normal to the plane of the substrate and the other two contained in it. The multiplicity of the fundamental reflection (220) is 3, whereas the multiplicity of the superlattice reflection (110) is 1, as can be seen from Figures 2(a) through (c). In other words, given the same degree of order in two samples exhibiting textures as in Figures 2(d) A and B, the detected intensity of (110) is 3 times lower in B than in A due to texture alone. Therefore, the experimentally detected intensities, which enter the numerator of Eq. [2], have to contain a correction factor as follows:

$$S_{3v} = \left(\frac{3 \cdot I_s/I_f}{I_s^0/I_f^0}\right)^{1/2} = \sqrt{3} \cdot S_{1v} \quad [4]$$

where S_{1v} was defined by Eq. [2]. The meaning of the subscripts $1v$ and $3v$ becomes clear now: S_{3v} is the order parameter, which incorporates the assumption about the c-axis being able to develop with equal probability along all three [001] variants. The orientation of the three variants is determined by the (100) faceting of the nanoparticles, being either perpendicu-

Table I. Multiplicities of Reflections and Theoretical Intensities in Electron Diffraction of the Fcc Disordered Reflections, Calculated with Eq. [3]

Plane	p_{random}	I_{random}	p_{110}	I_{110}	p_{100}	I_{100}	p_{111}	I_{111}
111	8	100	4	100	0	0	0	0
200	6	43.7	2	29.1	4	100	0	0
220	12	20.7	2	6.9	4	23.7	6	100
311	24	20.6	4	6.9	0	0	0	0
222	8	5.7	4	5.7	0	0	0	0
400	6	2.4	2	1.6	4	5.4	0	0
331	24	6.9	4	2.3	0	0	0	0
420	24	6.4	0	0	8	7.3	0	0
422	24	4.9	4	1.6	0	0	6	11.8

Table II. Theoretical Intensities in Electron Diffraction of the $L1_0$ Reflections in the Case of Perfect Order ($S = 1$), in the Random Orientation, and in Various Axial Textures, Calculated with Eq. [3]

Plane	p_{random}	I_{random}	p_{110}	I_{110}	p_{001}	I_{001}	p_{111}	I_{111}
001	2	16.34	2	32.59	0	0	0	0
110	4	12.99	2	12.96	4	42.39	2	96.46
111	8	100.00	4	100.00	0	0	0	0
200	4	30.65	0	0	4	100.00	0	0
002	2	13.28	2	26.49	0	0	0	0
201	8	5.31	0	0	0	0	0	0
112	8	3.52	4	3.51	0	0	2	13.07
220	4	7.30	2	7.28	4	23.82	2	54.20
202	8	13.47	0	0	0	0	4	100
221	8	1.72	4	1.72	0	0	0	0
003	2	0.38	2	0.75	0	0	0	0
310	8	1.42	0	0	8	4.62	0	0
311	16	14.31	0	0	0	0	0	0
113	8	6.36	4	6.35	0	0	0	0
222	8	5.69	4	5.68	0	0	0	0

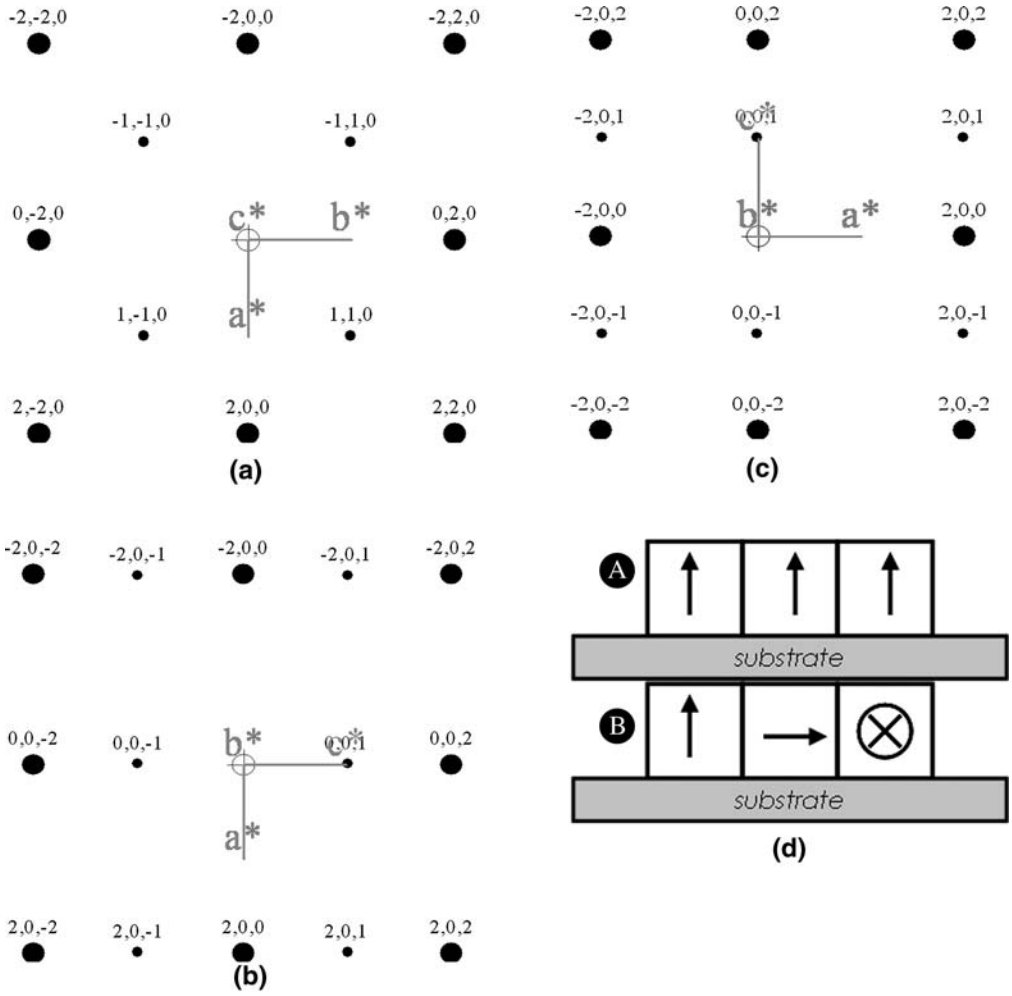

Fig. 2—The zone axes of the $L1_0$ structure corresponding to the orientations in (d): (*a*) [001] zone axis, (*b*) [010] zone axis, (*c*) another [010] zone axis, and (*d*) A: ideal [001] texture, single variant; B: ideal [001] texture in cubic nanoparticles, distributed uniformly among the three variants.

lar to the substrate or taking two perpendicular in-plane orientations. The term S_{1v} is the order parameter in the assumption of random orientation of the crystallographic planes with respect to the substrate. Information about the texture of the sample is provided by high-resolution TEM imaging. The choice for the definition of the order parameter as a function of texture is examined in Section IV.

III. EXPERIMENTAL RESULTS

Bright-field (BF) images of the as-prepared nanoparticle monolayers are shown in Figure 3. The as-prepared state is characterized by a fairly long-range assembly, where nanoparticles of 3.2 nm can be found in 1- to 10-μm size sixfold assemblies. The larger the particle size, the more difficult it is to obtain assemblies with large coherence lengths, such that the cubo-octahedral nanoparticles exhibit coherence lengths of the assembly of the order of 100 to 500 nm. Due to the nonunity aspect ratio of the particle dimensions and its variation, the 7.2-nm nanoparticles of cubic shape exhibit only local self-assembly. Most of the nanoparticles of cubic shape are rectangular prisms with an average minimum linear dimension (''width'') of 5.4 nm and an average maximum dimension (''length'') of 7.4 nm. Upon tilting the specimen by angles up to 50 deg, the aspect ratio of the dimensions does not change significantly. To define terms, the size of an assembly, or its coherence length, is the characteristic distance over which the assembly preserves its in-plane orientation. The coverage distance/area is the characteristic distance/area over which nanoparticles assemble, regardless of whether they preserve the coherence. Likewise, we refer to the shape of the nanoparticles as ''cubic'' when this is the case, and to the crystalline structure as fcc or fcc disordered to avoid confusion. ''Ordered'' is a descriptor reserved to denote the crystalline structure $L1_0$ and not the self-assembly.

Figure 4 presents the SAED patterns of the nanoparticles in the as-prepared, fcc disordered state. All SAED patterns are taken on monolayers, with the largest SA aperture of 5.6-μm diameter, comprising approximately 10^4 nanoparticles, except for the SAED pattern in Figure 4(c) for which a smaller aperture was used. By visual examination, it can be seen that the relative intensity of the (111) *vs* the (200) ring varies from sample to sample, which is an indication of texture. The 3.2-nm sample is closest to being randomly oriented, and the 7.2-nm sample is closest to being [001] textured. The amount of [001] texture is dependent on shape, and it roughly scales with particle size.

The texture was quantified by the ratio of intensities I_{111}/I_{200} and normalized to the theoretical ratio for random orientation, which can be calculated from column I_{random} of Table I as 2.288. A value of unity of the texture number ($t = 1$) signifies complete random orientation, and ($t = 0$) signifies perfect axial $<001>$ texture for our purpose. The absence of the (111) set of reflections from a diffraction pattern is not sufficient by itself to make us conclude which axial texture does the sample exhibit. However, high-resolution investigation of the nanoparticles as discussed here reveals prismatic shapes with facets oriented primarily along (100) planes in the 7.2-nm nanoparticles. The 3.2-nm nanoparticles exhibit a quasi-spherical shape with little faceting, and the 5.7-nm nanoparticles exhibit truncated cubo-octahedral facets along (100) and (111) planes. The texture of the nanoparticles in the as-prepared state and an annealed state of 650 °C for 2 hours is presented in Table III. The trend of increasing [001] texture with particle size can be observed as well as a tendency of randomization upon annealing.

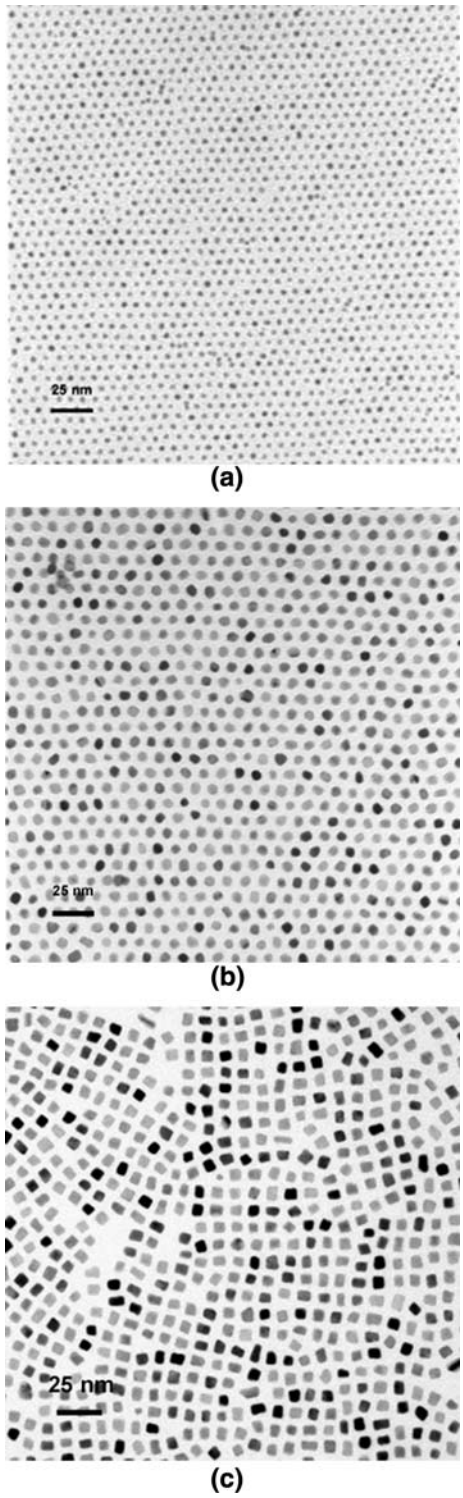

Fig. 3—Nanoparticles in the as-prepared state: (*a*) 3.2 nm, (*b*) 5.7-nm truncated cubo-octahedra, and (*c*) 7.2-nm cubes (image courtesy of Anup G. Roy, data storage systems center, Carnegie Mellon University, Pittsburgh, PA, USA).

Figure 5 shows the aspect of the monolayer after an annealing treatment of 2 hours at 650 °C. The annealing treatment preserved the coherence of the self-assembly

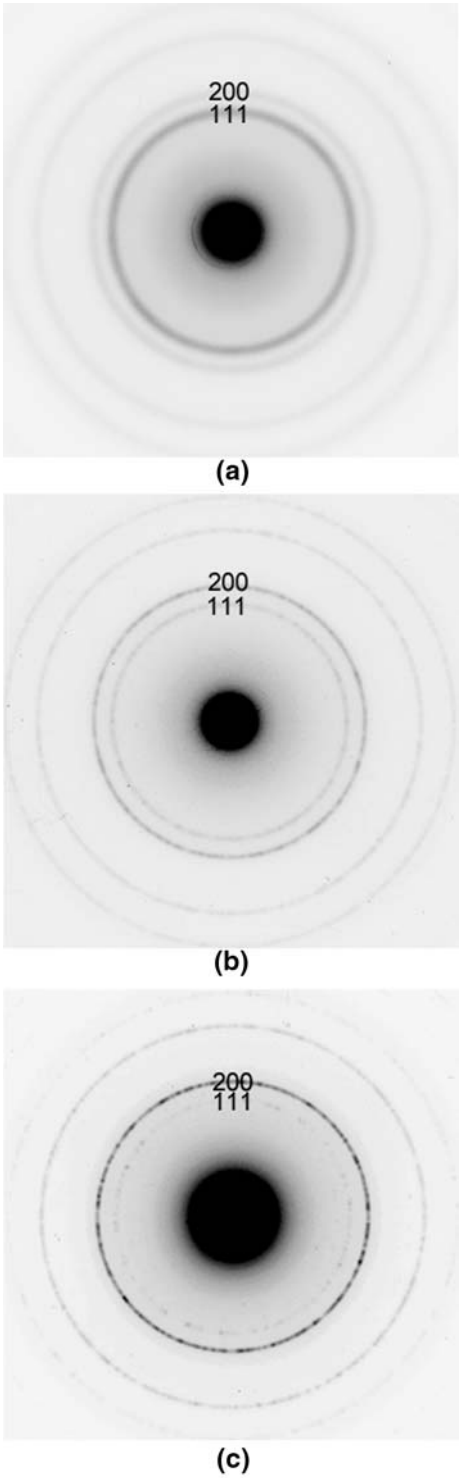

Fig. 4—Selected area diffraction patterns of the nanoparticles in the as-prepared state: (*a*) 3.2 nm, (*b*) 5.7 nm, and (*c*) 7.2 nm.

locally on areas no larger than 200 nm, as can be seen in Figure 6. Although the self-assembly was somewhat distorted, the particles remained sinter free on much larger areas so that medium (1.1 μm) and large (5.7 μm) selected area apertures could be used in taking the SAED micrographs. Figure 7 shows the development of the superlattice rings in the three particle sizes studied, on sinter-free monolayers. The superlattice (110) ring can be observed in each of the Figures 7(b) and (c).

Table III. Texture Number Calculated as $t = \frac{1}{2.288} \cdot I_{111}^{exp} / I_{200}^{exp}$

Theoretical Random Orientation	3.2 nm	5.7 nm	7.2 nm
1	0.6	0.3	0.1
Annealing 650 °C for 2 h	1	0.4	0.2

A. *Texture and Its Evolution during Annealing*

Although the superlattice ring (110) appears in annealed samples of all three sizes, it may be difficult to observe visually in Figure 7. Integrated-intensity diffraction patterns collected with a CCD camera are more useful for both qualitative observations and the quantitative determination of the order parameter. Figure 8(a) shows the integrated-intensity SAED patterns of the as-prepared samples, obtained by subtraction of the substrate contribution from the raw SAED signal, as shown in Figure 1(b). The dotted vertical lines mark the position of the first four fcc peaks, namely, (111), (200), (220), and (311). All samples have the fcc structure with a lattice parameter a = 3.85 Å. The relative intensity of the (111) *vs* (200) peak as a function of size can be observed in Figure 8(a), just as in Figure 4, and is indicative of texture, as described in Table III. The full-width at half-maximum of the peaks correlates with the particle size in a manner similar with the Scherrer formula for X-rays, and qualitatively it can be seen that the 3.2-nm sample has the broadest peaks, indicating the smallest particle size. In Figure 8(b), integrated-intensity SAED profiles from the 7.2-nm sample in the as-prepared state and annealed at two different temperatures are presented. The intensities were scaled such that the (200) peak has approximately equal height in all three graphs. Upon annealing, the fundamental peaks shift toward larger wavevectors monotonously with the annealing temperature, due to the development of the tetragonal $L1_0$ phase with $c < a$. The $L1_0$ peak (110) gradually develops and has the largest intensity for the highest annealing temperature. In the sample annealed at 650 °C for 2 hours, a tetragonal (002) peak of small intensity is also visible. The peak width stays constant before and after annealing, which confirms the absence of sintering, as shown in BF (Figure 5). The order parameters obtained are listed in Table IV.

B. *High Resolution to Determine Texture and Ordering*

In the literature, there are numerous reports on the observation of the disordered fcc structure and faceting in very small nanoparticles (3 nm), and a comprehensive review can be found in Zhang et *al.*[23] Our HREM observations confirm these findings and are not reiterated here. We are interested in ascertaining how the phase transformation fcc $\rightarrow$ $L1_0$ occurs in small nanoparticles, whether it is homogeneous or heterogeneous (as is the case for the bulk) and if a "critical size for

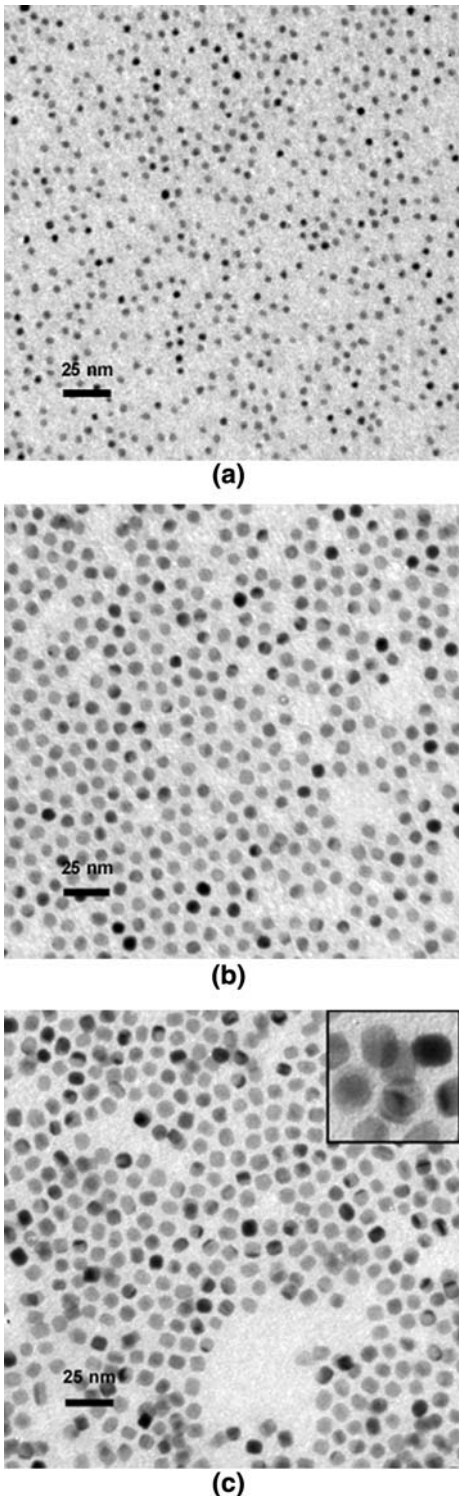

Fig. 5—Nanoparticle monolayers after an anneal at 650 °C for 2 h: (*a*) 3.2 nm, (*b*) 5.7 nm, and (*c*) 7.2 nm. The inset in c shows a high-magnification image of nanoparticles in contact, which shows no neck formation. This is the typical case for these annealing conditions (not the best case).

ordering" exists at the nanometer scale. It is suggested in the literature[12,24] that very small nanoparticles with sizes close to the superparamagnetic limit (~3 nm for

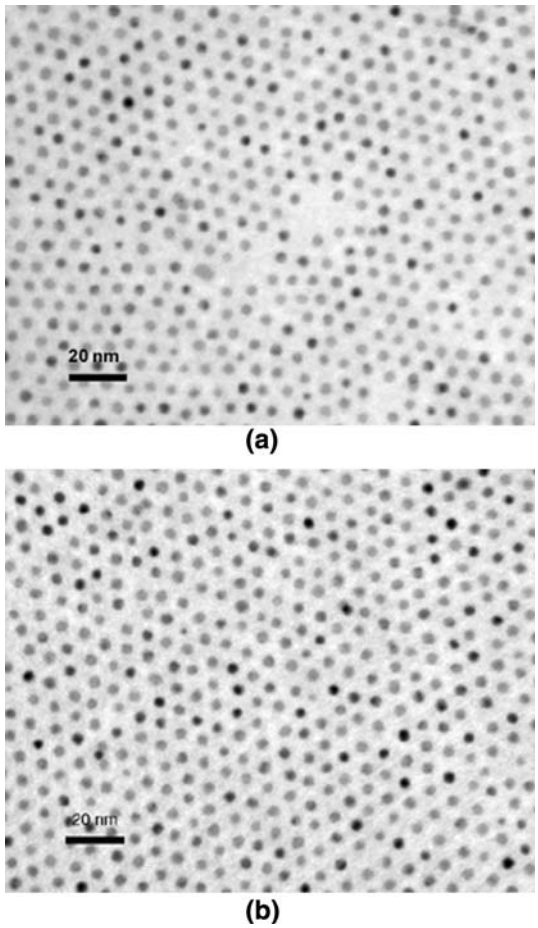

Fig. 6—The range in which the coherence length of the self-assembly is preserved in the case of 3.2-nm nanoparticle monolayers after an anneal of 600 °C for 1 h: (*a*) typical region and (*b*) best region (approximately 200-nm coherence length).

bulk FePt) either do not transform to the $L1_0$ phase or transform homogeneously.

From HREM evidence gathered during this study, 3.2-nm nanoparticles have been observed to order throughout the volume if they are single crystals. Such a particle is presented in Figure 9(a). It is known that as-prepared nanoparticles can exist in multiply-twinned states, and this state can be preserved after annealing. An ordered region may develop within one of these multiple twins, and an example is shown in Figure 9(b). In this image, only one ordered variant is imaged in the zone axis. A question can be raised here: whether this is a multiply-twinned structure originating in the disordered fcc state, in which one variant has ordered, or whether a region of the ordered phase has nucleated within the disordered fcc single-crystal matrix. Multiple twinned structures with one (or more) ordered variants cannot be taken as evidence of nucleation within 3.2-nm nanoparticles, because a structural variant is a single-crystal grain, which is found to be either disordered throughout or ordered throughout its volume. The convincing evidence for a heterogeneous transformation would be an $L1_0$ region, which has nucleated coherently within the fcc matrix of a single-crystal grain. No

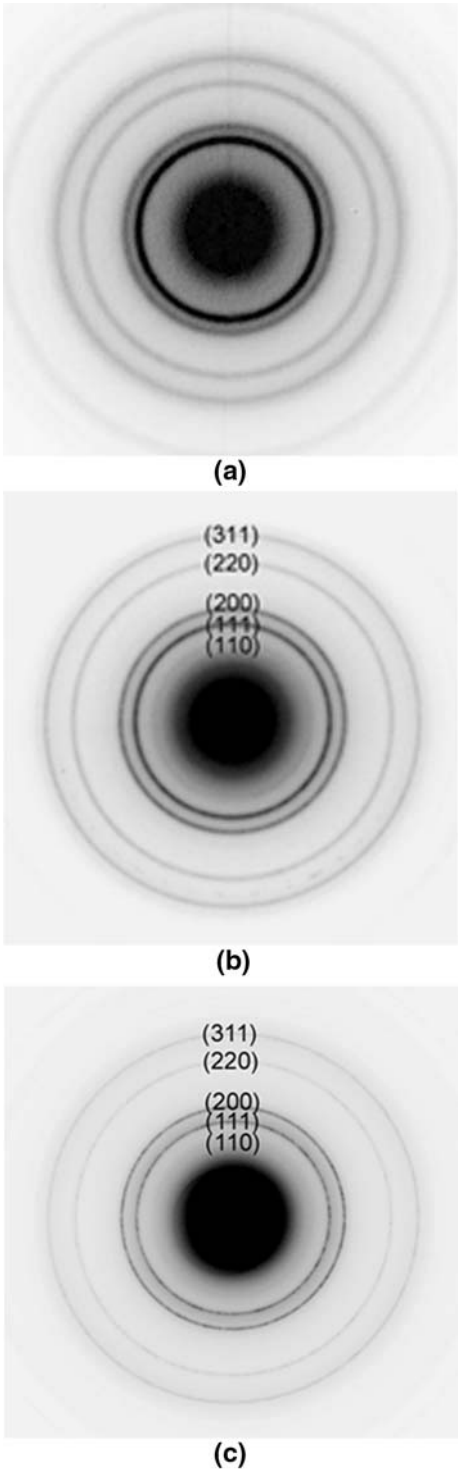

Fig. 7—SA diffraction pattern of nanoparticle monolayers after an anneal of 600 °C for 1 h: (*a*) 3.2-nm, (*b*) 5.7-nm, and (*c*) 7.2-nm nanoparticle monolayers after an anneal of 600 °C for 2 h.

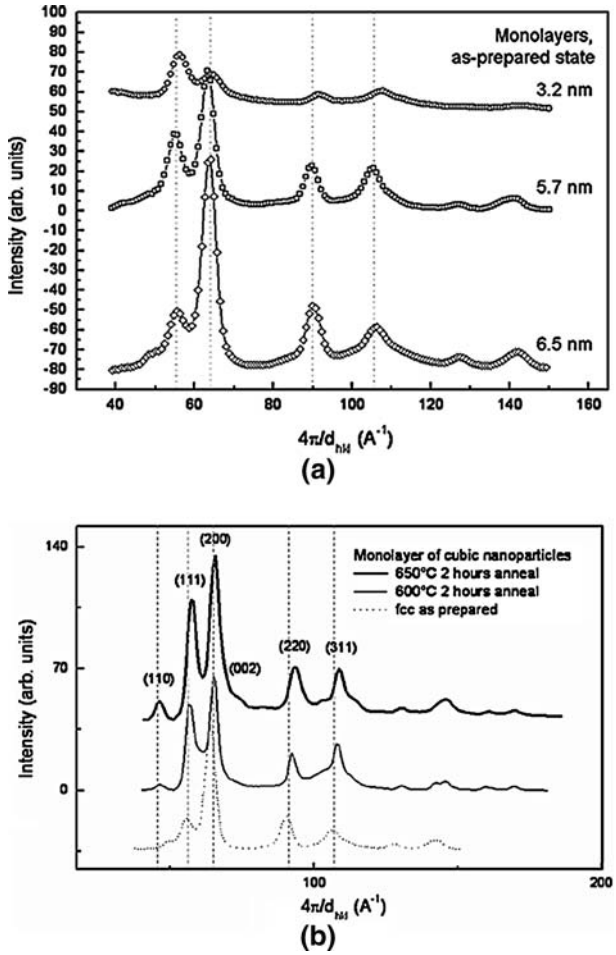

Fig. 8—(*a*) Integrated-intensity SAED patterns collected from monolayers of as-prepared, fcc disordered samples of three sizes. Vertical lines indicate the position of the peaks (111), (200), (220), and (311). (*b*) The emergence of the ordered phase in a 7.2-nm nanoparticle sample: the as-prepared fcc state (dotted line), annealed at 600 °C for 2 h (thin line), and annealed at 650 °C for 2 h (thick line). Vertical dotted lines indicate the position of (110) and the fcc peaks in (a).

evidence of coherent nucleation has been observed over the course of this study in 3.2-nm nanoparticles; therefore, we cannot draw a conclusion about the homogeneous/heterogeneous nature of the transformation in 3.2-nm nanoparticles.

However, the next larger size of nanoparticles (5.7 nm) sometimes displays the characteristics of a nucleation and growth transformation. Figure 10 shows two examples: a nucleus of the ordered phase embedded coherently within the fcc matrix is shown at left. The periodicity of the *c*-axis can be seen in the figure, and the fact that the nucleus has developed with the *c*-axis lying in the plane of the image can be seen by measuring fringe periodicities. The *c*-axis periodicity is the double of the fringe periodicity exhibited by {100} planes of the fcc matrix, which is $a/2$. In Figure 10(b), three [001] variants of the $L1_0$ phase can be seen within a 5.7-nm nanoparticle, two of them being similar. A fourth variant is oriented with the *c*-axis parallel to the electron beam, and its *c*-axis periodicity cannot be imaged. These variants cannot originate in the fcc phase and can only be the consequence of postpreparation annealing. They are a characteristic feature of the ordering transformation and are formed by the *c*-axis taking either of the three unit cell directions available in the as-prepared, single-crystal fcc matrix.

Table IV. The Order Parameter in the Three Different Particle Sizes Studied, Calculated with Eqs. [2] and [4]

Size	Anneal	S_{1v}	S_{3v}
3.2 nm	600 °C, 2 h	0.2	n/a
	650 °C, 2 h	0.3	n/a
5.7 nm	600 °C, 2 h	0.4	–
	650 °C, 2 h	0.5	–
7.2 nm	600 °C, 2 h	0.4	0.6
	650 °C, 2 h	0.6	0.9

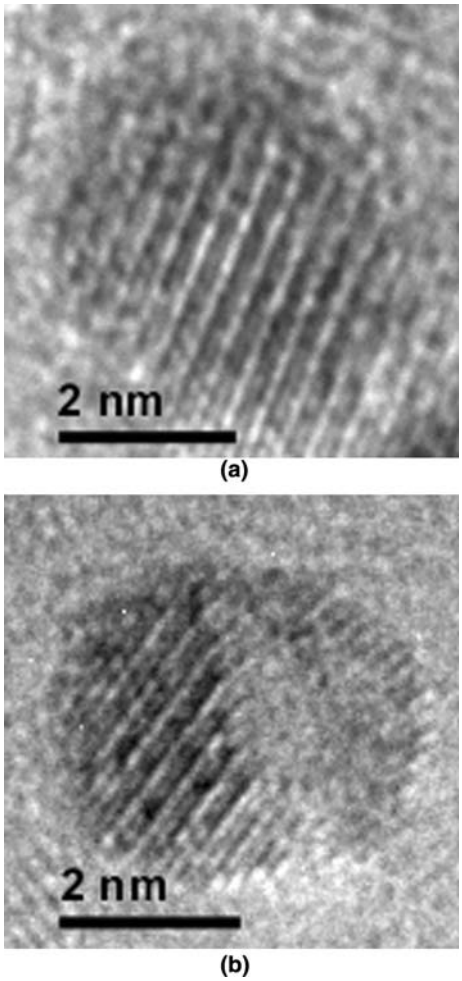

Fig. 9—The 3.2-nm nanoparticles annealed (*a*) at 650 °C for 30 min (superlattice reflection (001) fringes can be seen across the entire particle) and (*b*) at 650 °C for 10 min. Superlattice (001) fringes can be seen in the lower left half of the particle.

A fast Fourier transform analysis reveals the zone axes present in Figure 10(b) and their relative orientation. Figures 11(a) through (c) show the zone axes of each of the three variants in their relative orientation. The fast Fourier transform of the entire particle showing the superposition of the three zone axes is shown in Figure 11(d). An inverse Fourier transform selecting the pair of reflections 1 through 3 from Figure 11(d) yields Figure 11(e), which reproduces the fringe periodicities of the variants in the experimental image Figure 10(b).

The 7.2-nm nanoparticles exhibit pronounced (100)-type faceting in high resolution, which strongly supports the hypothesis of shape-driven texture. Nanoparticles are in contact with the substrate along their geometrical facets, which coincide with low-index crystallographic planes of either the fcc or the $L1_0$ structure. In the nanoparticles of cubic shape, the facets are {100} and the largely predominant zone axis orientation is <100> as well. Figures 12(a) and (b) show the most frequently encountered zone axis [100] in 7.2 nm cubic nanoparticles. This can be seen from the square pattern of the lattice fringe periodicity. They are parallel with the side faces of the nanoparticles, which indicates that these are (100)-type planes as well. The 5.7-nm cubo-octahedral nanoparticles produce an intermediate state of texture between the randomly oriented 3.2-nm particles and the [100]-oriented cubic particles. Although the [100] zone axis can be imaged in HREM with a higher frequency in cubo-octahedral particles than in 3.2-nm particles, the correlation between orientation and faceting is not as straightforward as in the case of larger 7.2-nm cubic nanoparticles. The presence of facets of the type (100), (111), and (110) leads to a more complex combination of multiple axial textures. In Figure 12(a), (111)-type facets can be distinguished in the corners of the cube, making a 45 deg angle with the (100) plane periodicity fringes.

IV. DISCUSSION

A. *Shape and Texture*

This study focuses on the results of annealing using our procedure, which inhibits the sintering of nanoparticles in terms of agglomeration and grain growth, rather than in terms of the degradation of the self-assembly, which was observed but was not studied systematically. Care has been taken in all cases to encompass only monolayers in the selected area aperture of the electron microscope during our investigation of the ordering process. The absence of sintering was verified on the entire area comprised within the aperture prior to taking SAED micrographs.

While the 3.2- and 5.7-nm nanoparticles generally exhibited good self-assembly over large areas, the cubic-shaped nanoparticles of 7.2 nm exhibited occasional two- and three-particle agglomeration. The agglomeration propagates without significant change in the annealed states (Figure 5(c), see inset), and no neck formation is observed. By comparison of Figures 3(c) and 5(c), a slight change in shape can be seen. Whereas in Figure 3(c) the shapes are prismatic with well-defined corners, in Figure 5(c), the corners are rounded to minimize the surface energy. Because all images were taken after the samples were allowed to reach thermal equilibrium, we believe that this roughening is an indication that the as-prepared, cubic shapes are not equilibrium shapes, but that they are rather dictated by the kinetics of attachment of the surfactants to the facets during nanoparticle growth from solution. This conclusion is supported by the existence of previous reports of FePt nanoparticles in cubo-octahedral shapes by

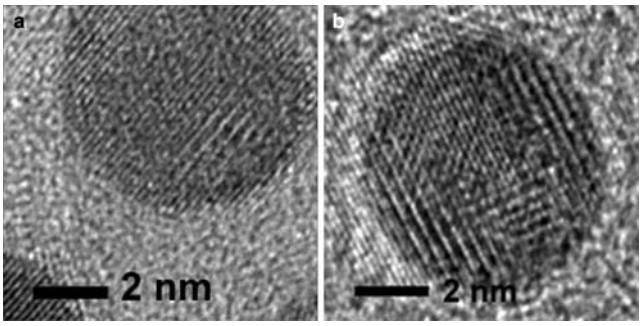

Fig. 10—Evidence of a heterogeneous phase transformation in 5.7-nm nanoparticles. Left: a small nucleated region of the $L1_0$ phase within the fcc matrix. Right: structural [001] variants of the $L1_0$ phase have developed after an annealing of 2 h at 600 °C.

varying the relative concentration of the surfactant.[14] It can be argued that the energy balance of the as-prepared nanoparticles implies the presence of surfactants, whereas that of the annealed nanoparticles does not, because the oleic acid/oleylamine mixture used as surfactant decomposes below 300 °C. However, we believe that the equilibrium shapes of surfactant-capped nanoparticles are largely determined by the same interatomic forces responsible for the equilibrium shapes of surfactant-free nanoparticles. Another interesting conclusion can be derived from the comparison between Figures 3(c) and 5(c). In the former image, the illumination within each nanoparticle is uniform, without contrast, and each nanoparticle appears either dark or light, corresponding to a single crystal oriented either in a zone axis or away from a zone axis. In the latter image, however, contrast within a single nanoparticle is frequently encountered, which is consistent with the reported observations of (111) annealing twins[14] and with (101) transformation twins, also called (001) variants. Development of variants during annealing explains the variable contrast within the cubic 7.2-nm nanoparticles. This, together with the development of (111) facets, as shown in Figure 12, explains the degradation of texture upon annealing, as seen in Table III. Although annealing permits the development of the $L1_0$ phase with large order parameters, the development of twin variants and additional facets acts against the preservation of the desired [100] axial texture, which is present in the as-prepared state.

B. *Order Parameter*

The work of Sato *et. al.*[25] comprises the order parameter determination for 8-nm-thick FePd nanoparticles annealed postdeposition at 873 K for up to 10 hours. They calculate the I_{110} and I_{220} intensities as a function of the order parameter in the assumption of dynamical scattering with the use of the multislice method and derive the order parameter from comparison with experimentally measured intensities. The definition of the order parameter used in their work is the measured ratio I_{110}/I_{220} corrected for thickness

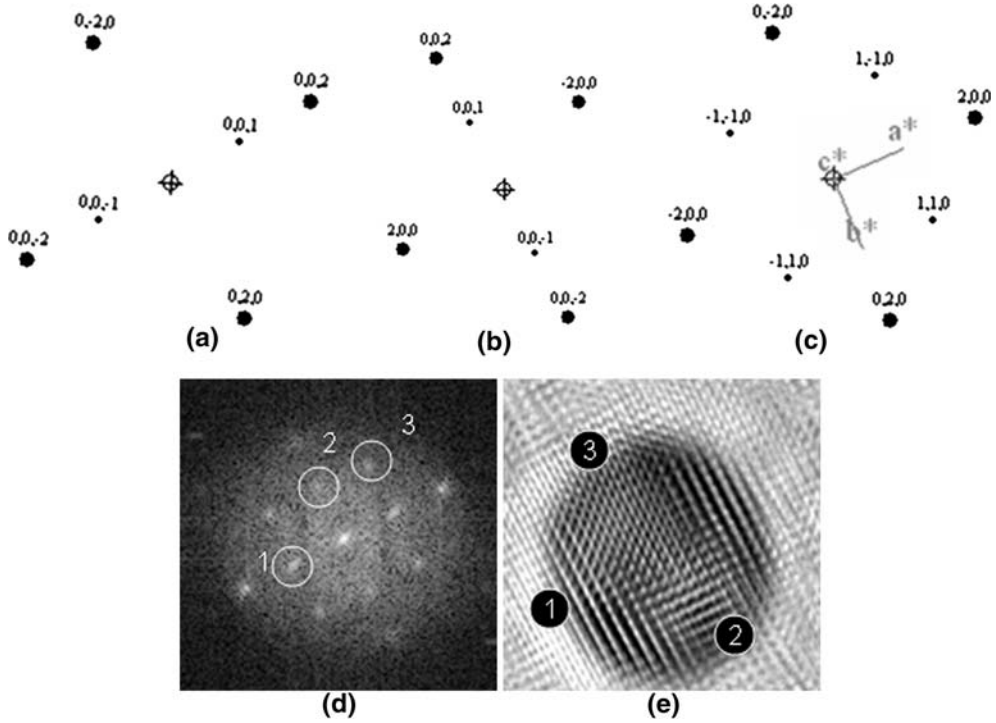

Fig. 11—Zone axis analysis for the structural variants present in Fig. 10 right: (*a*) zone axis [100], (*b*) zone axis [010], (*c*) zone axis [001], and (*d*) fast Fourier transform of Fig. 10 right. The superlattice reflections of each variant are identified as follows: reflection 1 is [100] type, reflection 2 is [010], and reflection 3 is [001]. (*e*) Inverse fast Fourier transform reconstruction of the nanoparticle using only the superlattice reflections [100], [010], and [001]. Numbers indicate the bright-field region reconstructed by each reflection.

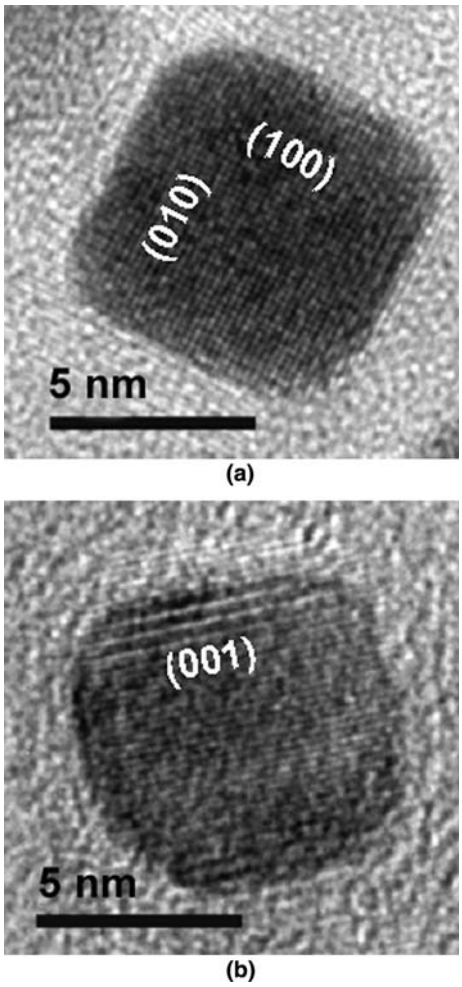

Fig. 12—(100) is the predominant zone axis encountered in 7.2-nm nanoparticles. Both images are taken from nanoparticles annealed at 600 °C for 2 h. (*a*) A [001] zone axis in which (100) and (010) lattice fringes can be seen. The corners are faceted along (111) planes. (*b*) The [001] direction lies in the plane of the image. (001) lattice fringes indicative of the $L1_0$ structure can be seen. In both cases, the {100} planes run parallel with the major facets of the sample.

effects, and they account for the Debye–Waller factor in their calculations. With our definition (2) for the order parameter, the evaluation of the Debye–Waller factor is not necessary, because the dependence of the diffraction angle $\sin\theta/\lambda$ cancels out by normalization to the fully ordered intensities I^0_{110}/I^0_{220}. The definition (2) of the order parameter also has the advantage of not having to account for size effects in the evaluation of B, which according to Sato *et. al.* (Reference 25 and References 22 through 26 therein) exhibits a strong particle size dependence and can affect up to 7pct the calculated value of the order parameter. However, the variation of B with size affects their long-range-order parameter values only in the second digit. Our calculations assume precision only up to the first digit due to the relatively limited sensitivity and resolution of the CCD camera, as opposed with the imaging plate system used in their study.

Of course, there is always the question of whether the kinematical approximation used in the calculation of the denominator of Eq. [2] applies to our experiment. Scattering can be considered kinematical when the diffraction intensities I_{hkl} of Eq. [3] amount to no more than a few percent of the transmitted beam intensity. The transition from kinematical to dynamical scattering occurs when

$$\lambda\left|\frac{\Phi_{hkl}}{\Omega}\right|\cdot t \approx 1 \qquad [5]$$

where λ is the wavelength of the electrons, Φ_{hkl} is the structure factor, Ω is the volume of the unit cell, and t is the thickness of the sample in the electron beam. An evaluation of this criterion for face-centered FePt using parameters $a = 3.816$ Å, an acceleration voltage of 120 kV, and the expression $\Phi_{hkl} = 2\left(f_{\mathrm{Fe},hkl} + f_{\mathrm{Pt},hkl}\right)$ for the structure factor gives $\Phi_{110} = 12.246$ Å, $\Phi_{220} = 6.3803$ Å, and the critical thickness for fcc FePt 13.6 nm for the (110) reflection and 26 nm for the (220) reflection. For an accelerating voltage of 200 kV, these values are, respectively, 18.1 and 34.7 nm. Because the largest particle size used in this study is 7.2 nm and we have only performed order parameter measurements on monolayers, we conclude that the kinematical approximation is a safe assumption for our calculations.

C. *Microstructure*

One of the purposes of this study was to ascertain whether the phase transformation occurs homogeneously or heterogeneously in the sense of Gibbs[26] in very small nanoparticles and what is the critical size for the phase transformation. It is possible that the Gibbs classification in homogeneous and heterogeneous transformations loses some meaning in very small nanoparticles, where the spatial extent available for the transformation is limited to the particle size, and the degree of fluctuations is limited by the atomic configuration over a few lattice parameter lengths. From estimations of the speed of growth of the ordered phase in FePt thin films based on Berry and Barmak,[27] a 3-nm nanoparticle might order heterogeneously throughout its volume in a time interval of the order of 40 ms, which would have been difficult to detect experimentally in our observations. However, a signature of the heterogeneous transformation would be to encounter a particle with an ordered [001] variant of the $L1_0$ phase coherent with the fcc matrix. Incoherent ordered grains or twin variants of which one is ordered as shown in Figure 9(b) were not taken as a proof of heterogeneous phase transformation in our study. Single-crystal grains smaller than 3.2 nm, which were found to be ordered as in Figure 9(b), constitute examples that the critical size for ordering is lower than 3.2 nm due to the pre-existence of multiply-twinned structures in the as-prepared state. Multiple twins in 3.2-nm nanoparticles are in a crystallographic relationship; however, each of them is a single-crystal grain, which is encountered to be either disordered throughout, or ordered throughout, its volume over the course of this study. This does not constitute evidence that the phase transformation at

these scales is heterogeneous as is the case with bulk and large-grained thin films (10 nm or more).

Our work fills in the gap in the literature on ordering of FePt nanoparticles in that it develops a method of preserving a strict size monodispersity upon annealing in monolayers, which we prove both directly[†] (by imaging) and indirectly (by diffraction). Electron diffraction also serves as a tool for measuring the texture and the order parameter of large ensembles comprising 10^3 to 10^4 nanoparticles. Similar work using X-ray diffraction either limits the annealing time to avoid sintering effects or shows slight sharpening of the diffraction peaks due to sintering and grain growth (for example, References 10 and 11, among recent articles). Removing the sintering effect during the phase transformation also allows a more accurate study of the order parameter evolution as a function of size and annealing temperature, confirming experimental[13] and theoretical[28] predictions of the depression of the transformation temperature in small nanoparticles. As a notable result, chemical order was demonstrated within variants of 3-nm monodispersed nanoparticles pushing the theoretical limit of the critical size for ordering in FePt below 3 nm. Compelling evidence of the critical particle size for the fcc $\rightarrow$ $L1_0$ phase transformation in nanoparticles is still lacking, and further investigation about the superparamagnetic character at these small sizes is required.

[†]A bright-field image of a monolayer exhibiting monodispersity upon annealing at 600 °C for 2 h was taken at the lowest magnification at which nanoparticles could still be distinguished. The purpose of this image is to show that preservation of monodispersity is controllable and not just a random, local effect.

V. CONCLUSIONS

We have studied the phase transformation fcc $\rightarrow$ $L1_0$ in FePt monodispersed nanoparticles of three different sizes between 3.2 and 7.2 nm with a tight size distribution, employing a novel sinter-free annealing procedure. The texture and the order parameter of nanoparticle monolayers were determined quantitatively using the azimuthally integrated electron diffraction signal collected with a CCD camera. The discontinuous character of the phase transformation was established for nanoparticles of 5.7-nm average diameter and larger.

The order parameter in all nanoparticle sizes exhibits a monotonous dependence on the annealing temperature. Close to 1 degree of order in the absence of sintering can be achieved in {001} textured 7.2-nm nanoparticles at 650 °C after 2 hours, with some degradation of texture. The same trend of the degradation of texture can be observed in smaller 3.2- and 5.7-nm nanoparticles, which exhibit correspondingly smaller order parameters.

We have not found a critical size for ordering in FePt, even at sizes as small as 3.2 nm, in the presence of a carbon nitride overcoat. If such a critical size exists, it should depend on the nature of the embedding matrix for nanogranular thin films,[13] or on the nature of the overcoat for nanoparticles. Annealing at 600 °C and 650 °C showed that the highest order parameter for a given set of annealing conditions depends on the particle size and is largest for the largest particle size. This dependence of the order parameter on the particle size confirms previous predictions of the depression of the ordering temperature with size in the 3- to 10-nm range.[28,29,30]

ACKNOWLEDGMENTS

This research is sponsored by the Data Storage Systems Center of Carnegie Mellon University and by Seagate Research. We thank N.T. Nuhfer for the microscopy support and insightful discussions. The submitted manuscript has been created by Uchicago Argonne, LLC, Operator of Argonne National Laboratory (“Argonne”). Argonne, a U.S. Department of Energy Office of Science Laboratory, is operated under Contract No. DE-AC02-06CH11357. The U.S. Government retains for itself, and others acting on its behalf, a paid-up nonexclusive, irrevocable worldwide license in said article to reproduce, prepare derivative works, distribute copies to the public, and perform publicly and display publicly, by or on behalf of the Government.

ELECTRONIC SUPPLEMENTARY MATERIAL

The online version of this article (doi: 10.1007/s11661-006-9081-6) contains supplementary material, which is available to authorised users.

REFERENCES

1. S.H. Sun, C.B. Murray, D. Weller, L. Folks, and A. Moser: *Science*, 2000, vol. 287, pp. 1989–92.
2. H. Zeng, S. Sun, R.L. Sandstrom, and C.B. Murray: *J. Magn. Magn. Mater.*, 2003, vol. 266, pp. 227–32.
3. Z.R. Dai, S. Sun, and Z.L. Wang: *Nano Lett.*, 2001, vol. 1 (8), pp. 443–47.
4. Y. Ding, S.A. Majetich, J. Kim, K. Barmak, H. Rollins, and P. Sides: *J. Magn. Magn. Mater.*, 2004, vol. 284, pp. 336–41.
5. Min Chen: Ph.D. Thesis, University of Tuscaloosa, Tuscaloosa, AL, 2001.
6. M. Yu, Y. Liu, A. Moser, D. Weller, and D.J. Sellmyer: *Appl. Phys. Lett.*, 1999, vol. 75, pp. 3992–994.
7. T. Shima, T. Moriguchi, S. Mitani, and K. Takanashi: *Appl. Phys. Lett.*, 2002, vol. 80, pp. 288–90.
8. S.S. Kang, J.W. Harrell, and D.E. Nikles: *Nano Lett.*, 2002, vol. 2, pp. 1033–36.
9. Y. Sasaki, M. Mizuno, A.C.C. Yu, M. Inoue, K. Yazawa, I. Ohta, M. Takahashi, B. Jeyadevan, and K. Tohji: *J. Magn. Magn. Mater.*, 2004, vol. 282, pp. 122–26.
10. K. Elkins, D. Li, N. Poudyal, V. Nandwana, Z. Jin, K. Chen, and J.P. Liu: *J. Phys. D.*, 2005, vol. 38, pp. 2306–09.
11. L.E.M. Howard, H. Loc Nguyen, S.R. Giblin, B.K. Tanner, I. Terry, A.K. Hughes, and J.S.O. Evans: *J. Am. Chem. Soc.*, 2005, vol. 127 (29), pp. 10140–10141.
12. Y.K. Takahashi, M. Ohnuma, and K. Hono: *J. Appl. Phys.*, 2003, vol. 93 (10), pp. 7580–582.

13. Y.K. Takahashi, T. Koyama, M. Ohnuma, T. Okhubo, and K. Hono: *J. Appl. Phys*., 2004, vol. 95 (5), pp. 2690–96.
14. Z.R. Dai, S. Sun, and Z.L. Wang: *Surf. Sci*., 2002, vol. 505, pp. 325–35.
15. H. Zeng, P.M. Rice, S.X. Wang, and S. Sun: *J. Am. Chem. Soc*., 2004, vol. 126, pp. 11458–11459.
16. M. Chen, J.P. Liu, and S. Sun: *J. Am. Chem. Soc*., 2004, vol. 126, pp. 8394–95.
17. M. Chen, J. Kim, J.P. Liu, H. Fan, and S. Sun: *J. Am. Chem. Soc*., 2006, vol. 128, pp. 7132–33.
18. N. Shukla, C. Liu, and A.-G. Roy: *Mater. Lett*., 2006, vol. 60, pp. 995–98.
19. J.L. Lábár: *Ultramicroscopy*, 2005, vol. 103, pp. 237–49.
20. M. Tanase: Ph.D. Thesis, Carnegie Mellon University, Pittsburgh, PA, 2005.
21. B.E. Warren: *X-Ray Diffraction*, Addison-Wesley Publishing Company, Reading, Massachusetts, 1969.
22. B.K. Vainshtein: *Structure Analysis by Electron Diffraction*, Pergamon Press, New York, NY, 1964.
23. J. Zhang, Z.-L. Wang, J. Liu, S. Chen, and G.-Y. Liu: *Self-Assembled Nanostructures*, Nanostructure Science and Technology Series, Kluwer Academic/Plenum Publishers, New York, 2003.
24. N.T.J. Klemmer, C. Liu, N. Shukla, X.W. Wu, D. Weller, M. Tanase, D.E. Laughlin, and W.A. Soffa: *J. Magn. Magn. Mater*., 2003, vol. 266 (1–2), pp. 79–87.
25. K. Sato, Y. Hirotsu, H. Mori, Z. Wang, and T. Hirayama: *J. Appl. Phys*., 2005, vol. 97 (8), pp. 084301 1–084301 7.
26. J.W. Gibbs: *Trans. Connecticut Acad*., vol. III, pp. 108–248, Oct. 1875–May 1876 and pp. 343–524, May 1877–July 1878.
27. D.C. Berry and K. Barmak: *J. Appl. Phys*, 2006, vol. 99, pp. 08G901-1–08G901-3.
28. B. Yang, M. Asta, O.N. Myrasov, T.J. Klemmer, and R. Chantrell: *Scripta Mater*., 2005, vol. 53 (4), pp. 417–22.
29. H. Yasuda and M. Mori: *Z. Phys. D*, 1996, vol. 37, pp. 181–86.
30. Y.K. Takahashi, T. Okhubo, M. Ohnuma, and K. Hono: *J. Appl. Phys*., 2003, vol. 93, pp. 7166–68.